

Journal of
Mechanics of
Materials and Structures

**INVESTIGATING THE SECONDARY BUCKLING OF THIN FILMS
WITH A MODEL BASED ON ELASTIC RODS WITH HINGES**

Guillaume Parry, Christophe Coupeau, Jérôme Colin
and Alain Cimetière

Volume 4, N° 1

January 2009



mathematical sciences publishers

INVESTIGATING THE SECONDARY BUCKLING OF THIN FILMS WITH A MODEL BASED ON ELASTIC RODS WITH HINGES

GUILLAUME PARRY, CHRISTOPHE COUPEAU, JÉRÔME COLIN AND ALAIN CIMETIÈRE

Thin films are usually submitted to high residual compression stresses which cause them to delaminate and buckle. We focus on the case in which delaminated areas take the form of long rectangular strips. The most commonly observed buckling equilibria that develop on such strip-delaminated areas are the straight-sided wrinkle, the row of bubbles, and the telephone cord wrinkle. An analytical model, based on elastic rods with hinges and taking into account the contact between film and substrate, is set up for the study of the post-buckling regime of the transition from straight-sided wrinkles to bubbles. The existence of snap-through is investigated; previous numerical studies revealed that this phenomenon can sometimes occur. The present analytical approach excludes numerical artifacts that can easily arise due to the high sensitivity of this problem to initial imperfections. The model reveals a critical bubble aspect ratio associated with the snap-through, and the existence of several simultaneous bubble equilibria.

1. The thin film secondary buckling problem and its mechanical description

The mechanical behavior of stressed multilayers and thin films has been the object of several investigations over the past twenty years in the fields of solid mechanics [Hutchinson and Suo 1991; Moon et al. 2004; Evans and Hutchinson 2007; Tvergaard and Hutchinson 2008] and materials sciences [Gille and Rau 1984; Abdallah et al. 2008]. Coatings are involved in a wide range of technological applications from microelectronic devices to thermal barrier coatings used in aero-engines.

High residual compressive stresses tend to arise in thin films deposited on substrates. The stress levels can be high and can reach, for instance, a few GPa in the case of thin metallic films prepared by sputtering deposition methods. The films may consequently delaminate and buckle spontaneously under the effects of high stress. Delamination and buckling are closely related; buckling occurs on the delaminated areas of the film where the flat equilibrium shape is no longer stable. Many buckling shapes can be observed on a delaminated area depending on the area's shape and on the stresses present in the film.

In the present text, we shall focus our attention on equilibria developing on rectangular areas of infinite length, which we shall refer to as "strip-delaminated" areas. The most common buckling equilibria on such domains are the straight-sided wrinkle, the row of bubbles, and the telephone cord wrinkle. Evidence from experiment [George et al. 2002] and analytical theory [Audoly 1999] suggests that both the bubbles and the telephone cord equilibria can result from the buckling of the straight-sided wrinkle. In those studies the delaminated strip was modeled as a von Karman plate and the perturbation method was used on the straight-sided wrinkle. Since the straight-sided wrinkle is itself a post-buckling state of the flat film (a primary buckling), the two other equilibria are often referred to as "secondary buckling" equilibria. A

Keywords: mechanical properties of thin films, static buckling, instability, variational and optimizational methods, elastic rods with hinges models.

stability diagram of the different secondary buckling equilibria has been recently determined [Parry et al. 2006]. The boundaries of the stability domains of the different equilibria are associated with critical values of some nondimensional loading parameters, stress level, elastic properties, delaminated strip width, and film thickness. The delaminated strip was also modeled as a plate, and the stability domains have been obtained through finite element calculations, taking into account large displacements and the contact between film and substrate. This allows one to follow the buckled structure in the advanced post-critical regime. Investigation of these secondary buckling equilibria is still active [Jagla 2007; Gruttmann and Pham 2008; Song et al. 2008].

Numerical exploration by means of the finite element method has proved to be valuable for gaining a better understanding of thin film secondary buckling phenomena. It has enabled us to follow the post-critical paths far from the straight-sided wrinkle equilibrium [Parry et al. 2006]. Nevertheless, because it consists in following along equilibrium branches, using initial imperfections with shapes designed to guide the solution toward the desired equilibrium branch in the neighborhood of the bifurcation point, this type of exploration is “local” in the sense of the loading space: it does not offer a global vision and understanding of the whole equilibrium branch structure. For a given loading and for a chosen set of parameters, the exact number of possible branches (that is, of possible buckling states) is not known *a priori*. It is consequently possible to miss a bifurcation point or snap-through.

In this context, a simplified model based on elastic rods with hinges has been developed in order to study *analytically* the secondary buckling of the strip-delaminated structure, especially the transition from straight-sided wrinkle to bubbles. A two-parameter model, capable of characterizing the straight-sided buckle to bubbles transition, has been set up. Such simplified models have proved to be valuable in analyzing post-critical buckling phenomena [Thompson and Hunt 1973; Arboez et al. 1987]. The idea is to provide intrinsic characteristics of the transition, explicitly investigating the parameters’ dependence and avoiding numerical artifacts.

The equations derived from the simplified model have to be simple enough to be solved by analytical methods, or at least to involve only very basic numerical tools. In the meantime, the model has to be realistic enough to conserve the post-critical behavior of the original structure. As we will show, the simplified model fulfills the above requirements.

Although the model is simplified compared to the original thin film, it shows behavior similar to thin films, and, therefore, can help by giving some explanation of the buckling behavior for such films. The phenomena are qualitatively well reproduced, and the critical values (critical a/b ratio, critical load) can also be predicted quantitatively with good accuracy.

2. Experimental results for the strip-delaminated thin films buckling problem

In this section, we present experimental results for the uniaxial compression of nickel thin films on polycarbonate substrates leading to strip buckling patterns. A summary of the experimental observations related to secondary buckling patterns is made.

Recent experiments [Coupeau et al. 1998] have been carried out on nickel thin films deposited on polycarbonate substrates using *in situ* atomic force microscopy (AFM) imaging together with a compression device. Uniaxial compression of the substrate is performed, with two purposes (Figure 1).

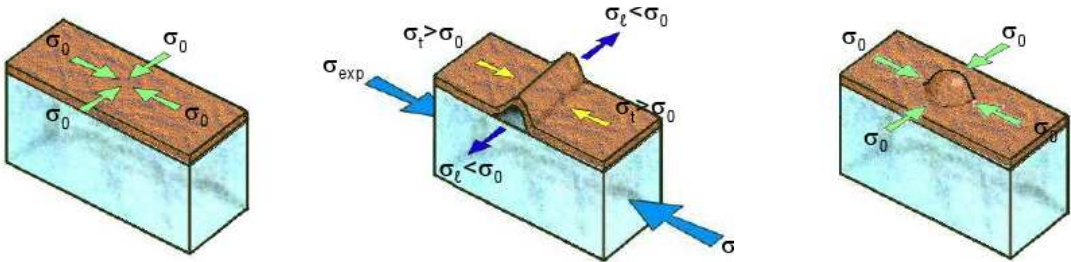


Figure 1. Uniaxial compression of a nickel thin film on a polycarbonate substrate. Left: Nickel thin film on polycarbonate substrate. Equibiaxial stress of magnitude σ_0 in the film. Middle: An uniaxial compression is applied to the substrate leading to strip-shaped delamination and straight-sided wrinkle formation. This structure is stable because of the high transversal compression. The small arrows indicate the stress variations in the film. Right: As the external compression is released, the straight wrinkle bifurcates into a row of bubbles. The stress state is back to the initial equibiaxial stress of magnitude σ_0 in the adherent parts of the film.

- The first purpose is to induce the strip-delamination pattern on the film; a network of parallel strips develops perpendicularly to the compression axis (Figure 1, middle; σ_{exp} is the stress induced in the substrate by the experimental device).
- The second purpose is to modify the initially equibiaxial stress state in the film (Figure 1, left), and hence the loading applied to the delaminated strips. The variation of the stress state in the film due to external compression is depicted in the middle part of the same figure.

Denote by σ_t and σ_l the stress components in the adherent part of the film, taken in the transversal and longitudinal directions of the strip, respectively (these are principal values, as the compression direction is perpendicular to the strips). The loading applied to the delaminated part of the film is in fact a displacement prescribed by the substrate along the boundaries of the delaminated area. The values σ_t and σ_l are directly related to this imposed displacement.

Before applying external compression, the film is only submitted to an equibiaxial compression state due to the internal stress ($\sigma_t = \sigma_l \equiv \sigma_0$) (first and left parts of Figure 1). During the uniaxial compression of the substrate, the stress component in the film becomes more compressive in the compression direction (that is, in the transversal direction of the strip) whereas the stress component perpendicular to the compression direction (that is, in the longitudinal direction of the strip) becomes *less* compressive (middle part of same figure). This behavior results from the difference between the Poisson's coefficients of the two materials ($\nu_{\text{film}} < \nu_{\text{substrate}}$). The ratio of stress components in the longitudinal and transversal directions of the strip (σ_l/σ_t) is a critical parameter which triggers the transition between the straight-sided equilibrium and the secondary buckling equilibria (bubbles or telephone cord).

Secondary buckling occurs while the external compression is released (Figure 1, right). As a matter of fact, a large external compression promotes a transversal stress component higher than the longitudinal one, leading to a stable straight-sided wrinkle (Figure 1, middle). While the external compression is released, the σ_l/σ_t ratio increases, destabilizing the straight-sided wrinkle and a bubble or telephone cord equilibrium then arises.

The only irreversible step of the experiment is the delamination of the interface, which determines the width of the strips during the first compression. The buckling itself is purely elastic (reversible) and the experiment can be repeated with multiple cycles. It is worth noting that the delaminated strip width does not evolve during the successive loading/unloading. The interaction of debonding with buckling of the film is not studied in this article. Many studies on this topic have been published (for example see [Thouless et al. 1992; Faulhaber et al. 2006]).

The reversibility of buckling in the above described experiment allows one to observe, in-situ, different areas of the film and to follow the different equilibria in their post-critical regime while the external compression is modified. Remarkable observations are:

- (a) both bubbles and telephone cords can be found on the same sample;
- (b) the transition from straight-sided wrinkle to bubbles is characterized by snap-through under particular conditions;
- (c) some bubbles are rather shallow, remaining on top of the straight-sided wrinkle, whereas others are much deeper, settling down to the substrate level, as observed in Figure 2.

These experimental observations reveal the strong nonlinear character of the problem. Transitions occur in configurations where large out-of-plane displacements are involved. The film-substrate contact is a source of nonlinearity as well. The wrinkle-to-bubbles transition is thus particularly complex.

The questions arising in point (a) were addressed in [Parry et al. 2006]. It was found that, for a given loading, bubbles tend to appear on the narrowest strips whereas telephone cords develop on wider ones.

The question pointed out in point (b), the snap-through in the wrinkle-to-bubbles transition, has been explored in [Parry et al. 2005] by means of the finite element method. The length-over-width ratio for the bubbles turns out to be a critical parameter for the nature of the transition.

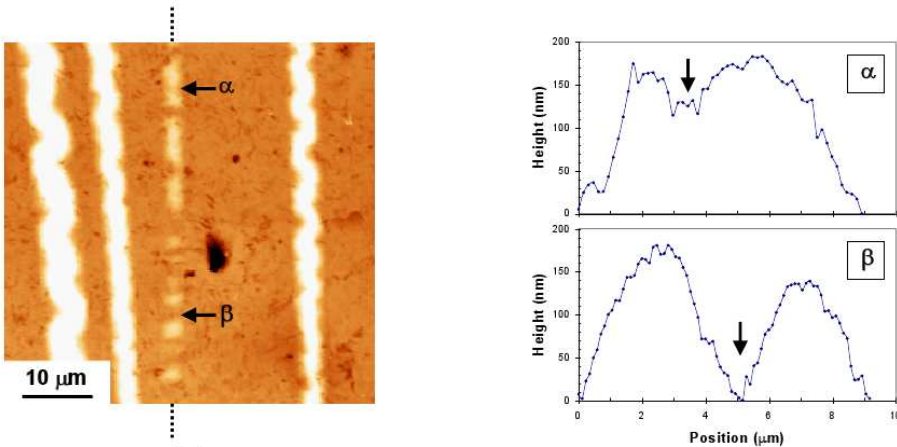


Figure 2. AFM image of a row of bubbles. Left: Detail of a row formed after the collapse of a straight-sided wrinkle. The other wrinkles in the neighborhood have a telephone cord buckling pattern. Two points are spotted, both located between two successive bubbles. Right: A slight depression is observed at point α , whereas the film is completely redeposited on the substrate at point β .

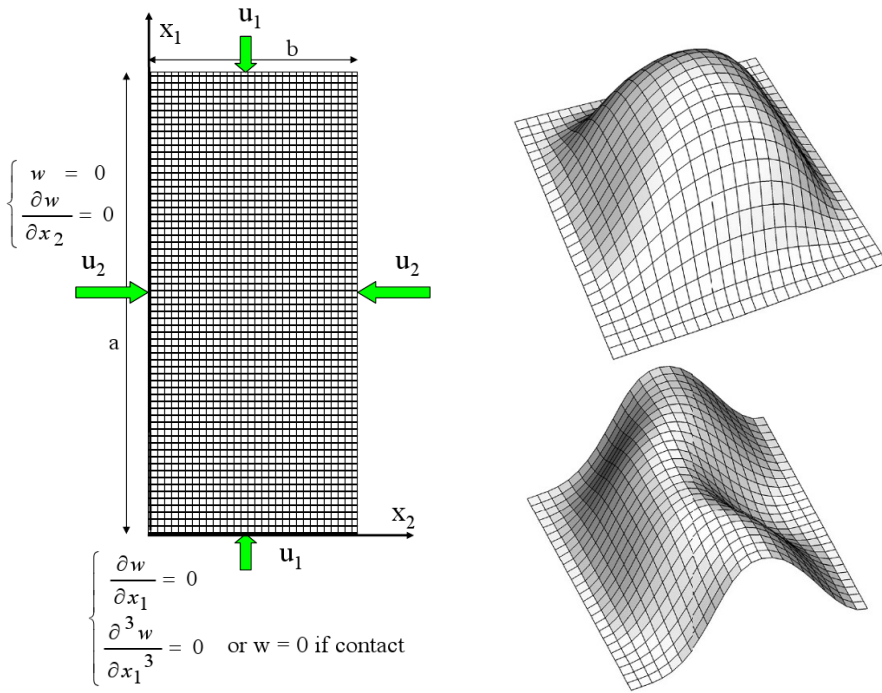


Figure 3. Structure sensibility to initial imperfections. Left: Mechanical model used in finite element computations. One unit cell (length a , width b) of the delaminated strip is modeled as a plate, with prescribed displacements at edges. Initial shape imperfection is on the order of $b/1500$. The straight-sided wrinkle bifurcates into a bubble structure (top right), or into a telephone cord structure (bottom right).

The two principal aims of the simplified model are to investigate point (c), which has not been addressed previously, and to explore further point (b). The latter point is difficult to address using plate theory and numerical methods because of the multiplicity of parameters and sensitivity of the secondary buckling to initial imperfections.

An example of this sensitivity is illustrated in Figure 3. In this example, a plate of length a and width b relies on a rigid support (Figure 3, left). The plate is submitted to displacements along its boundaries. The displacement components are normal to the plate edges. This plate represents one unit cell of the buckling mode: b is the strip width and a is the length of one bubble or the telephone cord spatial period. Two buckling calculations are carried out using two different initial geometric imperfections. The imperfections are very small, their amplitude being on the order of $b/1500$. In the first calculation (Figure 3, right top), the imperfection shape is “symmetric”, imitating a bubble. As the amplitude of the prescribed displacement increases, the plane structure first bifurcates in a straight-sided wrinkle; the secondary buckling under a bubble shape then occurs. In the second case (Figure 3, right bottom), an “antisymmetric” imperfection inspired by the telephone cord shape is introduced; the structure follows the same evolution as the process just described, from the plane structure to the straight-sided buckle,

but it finally bifurcates into a telephone cord shape as the loading is increased. These calculations show the key dependence of the numerical results on the initial imperfection used to carry out the calculation.

3. The simplified rod and spring model for buckling and post-buckling

The simplified system is composed of elastic rods, connected by hinges (Figure 4). The bending stiffness is obtained by introducing rotational springs between the rods. The arrows represent the prescribed load or displacement applied perpendicularly to the edges.

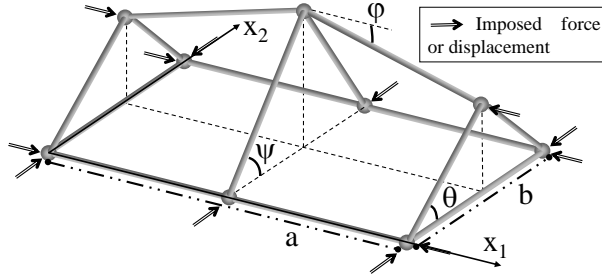


Figure 4. Rods and springs structure. The variables ψ , ϕ , and θ are the rotations of the rods with respect to the horizontal plane. The arrows stand for imposed forces or displacements.

The structure depicted in Figure 4 is one unit cell of width b and length a of the buckled structure that arises during secondary buckling. It represents a structure of spatial periodicity a , a straight-sided wrinkle, or a flat structure.

A state of deformation is characterized by two angular parameters ϕ and ψ . For convenience, a third parameter θ is introduced which is a function of the two degrees of freedom ϕ and ψ ($\theta \equiv \theta(\phi, \psi)$). When $\phi = 0$ and $\theta = \psi$, the straight-sided wrinkle can be recognized. The value $\theta = 0$ indicates the point at which the post-critical regime is advanced enough such that the bubble edges come in contact with the substrate. All the other values ϕ , ψ , and θ describe states that are in the post-critical secondary buckling regime. It is worth noting here that the telephone cord buckle cannot be described by this model. In order to do so, the introduction of one additional parameter is necessary which would not allow us to preserve the simplicity and the clarity of our statements. The present study focuses on the wrinkle-to-bubbles transition.

The potential energy V of the structure is defined as

$$V = E_{\text{el}}^b + E_{\text{el}}^s - W_{\text{ext}}, \quad (1)$$

where E_{el}^b is the bending elastic deformation energy, E_{el}^s the stretching elastic deformation energy, and W_{ext} the work of external forces. The bending part of the elastic deformation energy is composed of the following terms:

$$E_{\text{el}}^b = \frac{1}{2}C_1\psi^2 + \frac{1}{2}C_1\theta^2 + \frac{1}{2}C_2\phi^2 + C_3\phi(\psi - \theta), \quad (2)$$

where C_1 and C_2 are the pure bending stiffness coefficients associated with bending around the Ox_1 and Ox_2 axes, respectively, and C_3 is the shear stiffness coefficient. The shear energy is chosen to be the simplest polynomial that vanishes for $\varphi = 0$ and $\psi - \theta = 0$.

It is necessary to carefully choose these three coefficients to obtain a realistic behavior of the simplified model. In order to find the coefficients, the behavior of the bars system is identified with the behavior of a rectangular plate of same dimensions (length a and width b) at the onset of buckling. The identification of the critical loads, for a well chosen set of buckling modes, allows for the determination of the coefficients.

For this identification step, the structure is loaded in its initial (flat) plane by forces applied normal to the edges (see Figure 5). Denote by f the force per unit length of the structure edge, so the total load applied on an edge parallel to the x_1 direction is fa . This load is distributed on the four hinges, with $fa/4$ at the extremities and $fa/2$ in the middle (as suggested by the periodicity conditions). The same argument holds for the load applied along the edges parallel to the x_2 direction.

The two chosen buckling modes that we wish to use for identification are:

- The straight-sided wrinkle (Figure 5, left), characterized by $\varphi = 0$ (hence $\theta = \psi$), arising from the flat equilibrium. This buckling mode does not activate shear, and makes it possible to identify coefficients C_1 and C_2 .
- The bubble mode (Figure 5, right), arising from the flat equilibrium. This mode activates shear, and allows for the determination of C_3 .

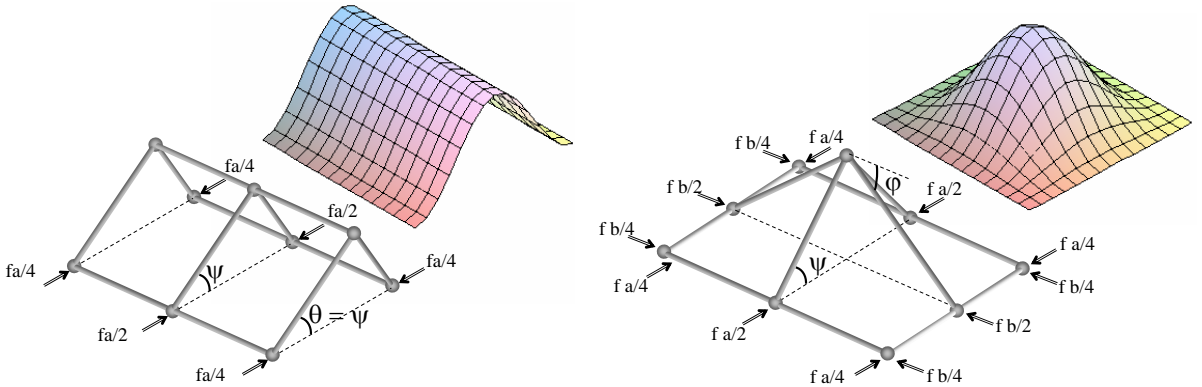


Figure 5. Buckling modes used for bending stiffness identification. Left: Straight-sided wrinkle mode. Right: Four times clamped plate or “deposited bubble” structure.

As the identification is made for incipient buckling, it is assumed that the deformation occurs without stretching of the middle plane. In this case, the potential energy of the bars structure is written as

$$V = \frac{1}{2}C_1\theta^2(\varphi, \psi) + \frac{1}{2}C_1\psi^2 + \frac{1}{2}C_2\varphi^2 + C_3\varphi(\psi - \theta(\varphi, \psi)) - 2\left(f\frac{a}{2}(1 - \cos\varphi)\frac{b}{2}\right) - 2\left(f\frac{b}{2}(1 - \cos\theta(\varphi, \psi))\frac{a}{2}\right) - 2\left(f\frac{b}{2}(1 - \cos\psi)\frac{a}{2}\right). \quad (3)$$

We now describe the first step of the identification process, that is, the determination of C_1 using the straight-sided wrinkle equilibrium (Figure 5, left). It is possible to find an exact solution of the von

Karman equation for this straight-sided wrinkle problem, for example, [Hutchinson and Suo 1991]. The critical value f_c of the force per unit length associated with this buckling mode is $f_c = 4\pi^2 D/b^2$ (with D the flexural stiffness of the plate). As far as the bars structure is concerned, this equilibrium is characterized by $\varphi = 0$ and $\theta = \psi$. The critical value of the load is $f_c = 2C_1/(ba)$. We deduce that

$$C_1 = 2\pi^2 D \frac{a}{b}, \quad C_2 = 2\pi^2 D \frac{b}{a}. \quad (4)$$

We next describe the second step of the identification process, that is, the determination of C_3 using the bubble equilibrium (Figure 5, right). There is no exact solution for the buckling problem of a rectangular plate clamped along all edges. Nonetheless, a good approximation for the solution to this problem is

$$w(x, y) = \frac{w_m}{4} \left(1 - \cos \frac{2\pi}{a} x\right) \left(1 - \cos \frac{2\pi}{b} y\right). \quad (5)$$

An approximate critical buckling load is obtained by setting the work of external forces ΔW equal to the bending energy ΔU_b of the plate for any amplitude w_m of the lateral deflection. These two expressions ΔW and ΔU_b can be written as

$$\begin{aligned} \Delta W &= \frac{1}{2} \int_0^a \int_0^b \left(f \left(\frac{\partial w}{\partial x} \right)^2 + f \left(\frac{\partial w}{\partial y} \right)^2 \right) dx dy, \\ \Delta U_b &= \frac{D}{2} \int_0^a \int_0^b \left(\left(\frac{\partial^2 w}{\partial x^2} + \frac{\partial^2 w}{\partial y^2} \right)^2 - 2(1-\nu) \left(\frac{\partial^2 w}{\partial x^2} \frac{\partial^2 w}{\partial y^2} - \left(\frac{\partial^2 w}{\partial x \partial y} \right)^2 \right) \right) dx dy, \end{aligned}$$

which provides the value for the approximate critical buckling load,

$$f_c = \frac{4\pi^2 D}{b^2} \frac{2\tilde{a}^2 + 3 + 3\tilde{a}^4}{3\tilde{a}^2(1 + \tilde{a}^2)}, \quad (6)$$

with $\tilde{a} = a/b$. Finite-element parametric studies show that this analytical formula for the bubble buckling load is quite accurate.

We now calculate the critical load associated with the system of bars. The potential energy given by equation (3) is used here. The relationship between the angles is $\sin \theta = \sin \psi - (a/b) \sin \varphi$, which under the small displacement hypothesis becomes $\theta = \psi - (a/b)\varphi$. The bubble equilibrium is characterized by $\theta = 0$. Taking into account these equalities yields

$$f_c = \frac{4\pi^2 D}{b^2} \frac{3C_3/(D\pi^2)\tilde{a}^2 + 3 + 3\tilde{a}^4}{3\tilde{a}^2(1 + \tilde{a}^2)}, \quad (7)$$

from which $C_3 = \frac{2}{3}\pi^2 D$ is identified.

4. The unilateral buckling problem with two degrees of freedom

The displacements along the delaminated areas of the film are in fact imposed by the substrate. Let us call u_1 and u_2 the two components of the displacement imposed on the edges of the strip (Figure 6, left). We introduce the notation $u_1 = \frac{1}{2}a\varepsilon_1$ and $u_2 = \frac{1}{2}b\varepsilon_2$, where ε_1 and ε_2 are the biaxial strains in the adherent part of the film, due to the substrate action. During loading, the lengths of the rods change as

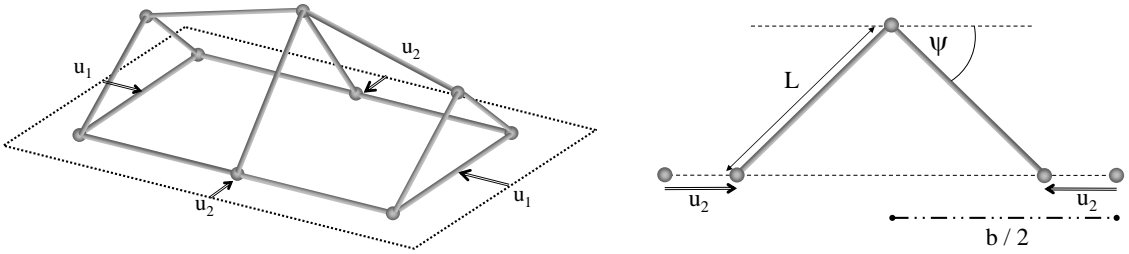


Figure 6. System of elastic rods under prescribed displacement. Left: Displacements u_1 and u_2 prescribed on the edges of the structure. Right: Relationships between displacement and current rod length.

illustrated in the case of the transversal rods, with rotation identified by the angular variable ψ in Figure 6, right.

In order to introduce the stretching energy component into the rod system, we have to identify an equivalent compression stiffness for each rod. This is done by matching the uniaxial compression stiffness of the rod system with that of a plate with the same dimensions. An illustration is given in Figure 7. The total compression force acting on the edge parallel to direction x_1 is $F = \sigma ha$. For a displacement ΔL of the edge, the stiffness of the plate is denoted K , with $F = K \Delta L$. Since $\sigma = E(2\Delta L/b)$, we identify $K = 2E(a/b)h$. This stiffness is distributed between the middle rod ($k' = E(a/b)h$) and the side rods ($k'' = \frac{1}{2}E(a/b)h$ for each rod, for symmetry reasons).

The same arguments hold for compression in the other direction (x_2 direction). The global stiffness is then $K = 2E(b/a)h$. It is distributed among the different rods as well.

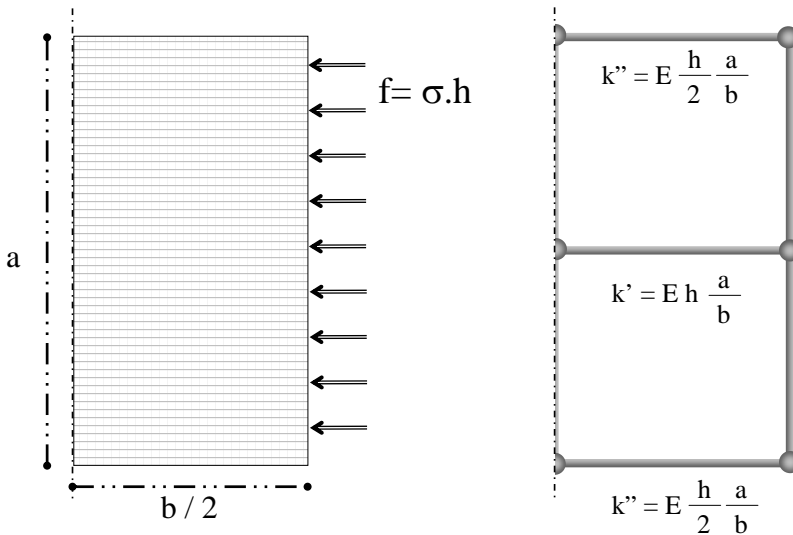


Figure 7. Rod-and-spring structure. The variables ψ , φ and θ are the rotations of the rods with respect to the horizontal plane. The arrows stand for imposed forces or displacements.

The next step is to express the length variation for each rod as a function of the angular variables. An example is depicted in [Figure 6](#), right, for the middle transversal rod which is associated with the rotation parameter ψ . The initial length for this rod is $b/2$. For a given value of ψ , the length L of the rod is given by $\frac{1}{2}b = L \cos \psi + u_2$. The length variation of the rod is

$$\Delta L = \frac{b}{2} \left(1 - \frac{1 - \varepsilon_2}{\cos \psi} \right).$$

The contact between the structure and the support, assumed to be rigid, is managed by the introduction of a reaction force, denoted R , exerted “upwards” by the support on the mobile lateral hinges ([Figure 8](#)).

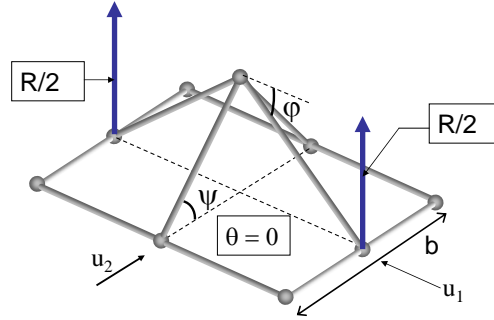


Figure 8. Contact force R due to the rigid support, applied to the central hinges when they come into contact with the support.

The vertical displacement d of a lateral hinge is linked to the lateral displacement and to θ by

$$d = \left(\frac{b}{2} - u_2 \right) \tan \theta = \frac{b}{2} (1 - \varepsilon_2) \tan \theta. \quad (8)$$

The displacement d and the reaction R satisfy the conditions

$$d \geq 0, \quad R \geq 0, \quad Rd = 0.$$

In order to take into account the unilateral contact, we introduce the potential energy of the system, which reads, in a nondimensional form $\tilde{V} = V/(\pi^2 D)$,

$$\begin{aligned} \tilde{V} = & \tilde{a}\theta^2 + \tilde{a}\psi^2 + \frac{1}{\tilde{a}}\varphi^2 + \frac{2}{3}\varphi(\psi - \theta) + \tilde{k}\tilde{a}\varepsilon_1^2 \\ & + \tilde{k}\tilde{a}\left(1 - \frac{1 - \varepsilon_1}{\cos \varphi}\right)^2 + \tilde{k}\tilde{a}\left(1 - \frac{1 - \varepsilon_2}{\cos \theta}\right)^2 + \tilde{k}\tilde{a}\left(1 - \frac{1 - \varepsilon_2}{\cos \psi}\right)^2 - \lambda d(\theta), \end{aligned} \quad (9)$$

where

$$\tilde{k} = \frac{Ehb^2}{4\pi^2 D}, \quad \tilde{a} = \frac{a}{b}, \quad \lambda = \frac{Rb}{2\pi^2 D}.$$

At equilibrium, λ and $d(\theta)$ satisfy the complementary conditions

$$\lambda \geq 0, \quad \lambda d(\theta) = 0.$$

In the following, we will omit the symbol \sim and handle only nondimensional values. Note that \tilde{k} expresses the competition between the stretching stiffness and the bending stiffness. Also note that the cosine terms account for the geometric nonlinearities. The notation $\varepsilon_1 = \rho\varepsilon$, $\varepsilon_2 = \varepsilon$ is introduced for the prescribed strains, with ρ , the biaxial prescribed displacement ratio.

5. Analysis of the equilibria

The rod system has two angular degrees of freedom, φ and ψ . The shape of the potential energy indicates that the underlying equilibrium equations of the systems are nonlinear. The equilibrium equations are solved for the rod system subjected to displacements $U = (u_1, u_2)$ as a simplified model for the delaminated film strip subjected to biaxial deformation $\varepsilon = (\varepsilon_1, \varepsilon_2)$. A sensitivity study of equilibrium stability with respect to the various parameters is carried out in order to characterize the transition from straight-sided wrinkle to bubbles.

The model experiment to which the results of this study can be compared is the previously described case of a 50 nm nickel thin film on a Polycarbonate substrate. A Young's modulus of 160 GPa has been experimentally determined for the film by using nano-indentation. The Poisson ratio is $\nu = 0.31$. The width b of the delaminated area is around $3 \mu\text{m}$. Using these data, a value of approximately 1000 is found for the parameter \tilde{k} .

Due to the fact that the substrate is relatively compliant compared to the film, the boundaries of the delaminated film can move slightly toward each other during delamination, leading to a relaxation in the direction x_2 (along the width of the delaminated strip). Hence ε_2 is smaller than ε_1 in the experimental case. The parameter ρ is set to 1.2 here in order to fit the non-equibiaxial loading conditions of the experiment.

The two variable parameters of the study are the aspect ratio of the unit cell a/b , accounting for the spatial periodicity of the bubble distribution, and the loading parameter ε , representing the level of compressive deformation prescribed by the substrate.

For each pair of parameters $(\varepsilon, a/b)$ a two-step procedure is carried out. The first step is the search of equilibria for which the system does not come into contact with the rigid support ($\theta > 0$, $\lambda = 0$). We will describe such equilibria as "contact-free". The second step is to check the existence of a contact equilibrium ($\theta = 0$, $\lambda > 0$). The potential energy can be computed for the different equilibria, and stability of the contact-free equilibria can be studied.

5.1. Search for contact-free equilibria ($\theta > 0$, $\lambda = 0$). We set $V_1(\varphi, \psi, \varepsilon) = V(\varphi, \psi, \lambda = 0, \varepsilon)$. The equilibrium equations for the contact-free equilibria are given by

$$\begin{aligned} \frac{\partial V_1}{\partial \psi} &= f_1(\varphi, \psi, \varepsilon) = 0, \\ \frac{\partial V_1}{\partial \varphi} &= f_2(\varphi, \psi, \varepsilon) = 0. \end{aligned} \tag{10}$$

The method consists in plotting the curves \mathcal{C}_1 and \mathcal{C}_2 representing $f_1 = 0$ and $f_2 = 0$, respectively, in the (φ, ψ) plane limited to the $(\psi \geq 0, \theta(\varphi, \psi) > 0)$ area for a given value of the loading parameter ε . Each couple of coordinates (ψ, φ) at an intersection point of the two curves corresponds to an equilibrium state.

Once a particular equilibrium (φ_1, ψ_1) has been identified, the Hessian matrix for the potential energy ($\partial^2 V / \partial u_i \partial u_j$ for $1 \leq i \leq 2, 1 \leq j \leq 2$) is computed with $u = (\varphi, \psi)$ in order to determine the shape of the potential energy in the neighborhood of equilibrium. The two eigenvalues, λ_1 and λ_2 , of this Hessian matrix are computed and their sign is analyzed.

- (a) If λ_1 and λ_2 are both strictly positive, the equilibrium is at a local strict minimum of the potential energy.
- (b) If λ_1 and λ_2 are both negative, the equilibrium is at a maximum of the potential energy.
- (c) If λ_1 and λ_2 have different signs, the equilibrium is at a saddle point of the potential energy.

Following the second variation stability criterion, only case (a) is associated with a stable equilibrium. As we shall see, two types of equilibria are discovered this way. The first one is the expected straight sided wrinkle (SSW) equilibrium, with $\varphi = 0$ and $\psi > 0$. The second one is a shallow-bubble (SB) equilibrium, with $\psi > \theta > 0$. This last equilibrium can represent experimentally observed equilibria that are characterized by shallow undulations at the top of SSW.

5.2. Search for contact equilibria ($\theta = 0, \lambda \geq 0$). Our model allows for the existence of a contact equilibrium subjected to a nonzero reaction force from the support ($\lambda > 0$). This is the representation of the deep-bubble (DB) equilibrium, experimentally observed when the film comes into contact with the substrate as bubbles form from the SSW equilibrium.

Write $V_2(\psi, \lambda, \varepsilon) = V(\varphi = (b/a)\psi, \psi, \lambda, \varepsilon)$. The equilibrium equations in the case of contact yield

$$\begin{aligned} \frac{\partial V_2}{\partial \psi} &= g_1(\psi, \lambda, \varepsilon) = 0, \\ \frac{\partial V_2}{\partial \lambda} &= g_2(\psi, \lambda, \varepsilon) = 0. \end{aligned} \tag{11}$$

For a particular set of values for $(a/b, \varepsilon)$, the solution to the above system indicates if a contact equilibrium exists (solution with $\psi > 0$ and $\lambda > 0$), as well as the value of ψ for the given equilibrium (that is, the bubble height).

5.3. Results. Three different post-critical behaviors can be identified, depending on the a/b ratio. We will address the problem of the equilibrium transition in light of three cases corresponding to the ratios $a/b = 0.9, 1$, and 1.1 . These cases are in the range of those observed experimentally. For each case, deformation levels from low to high are considered. Increasing the deformation level gives rise to new equilibria and can also trigger a change in the stability of those equilibria. The results are depicted in Figures 9, 10, and 11. Curves \mathcal{C}_1 and \mathcal{C}_2 have been drawn in solid and dashed lines, respectively. Each intersection point of the curves indicates the existence of an equilibrium. The trivial planar equilibrium ($\varphi = 0, \psi = 0$) and the SSW equilibrium ($\varphi = 0, \psi \neq 0$) are easily identified.

The potential V has also been plotted in each case in order to observe its shape in the neighborhood of each equilibrium. It is possible to see whether the equilibrium is a minimum, a maximum, or a saddle point of the potential, and hence to indicate its stability. Only the part where $\psi > \frac{a}{b}\varphi$ (that is, $\theta \geq 0$) is relevant. The other part shows the existence of a bilateral equilibrium, which is not possible here because of the rigid support.

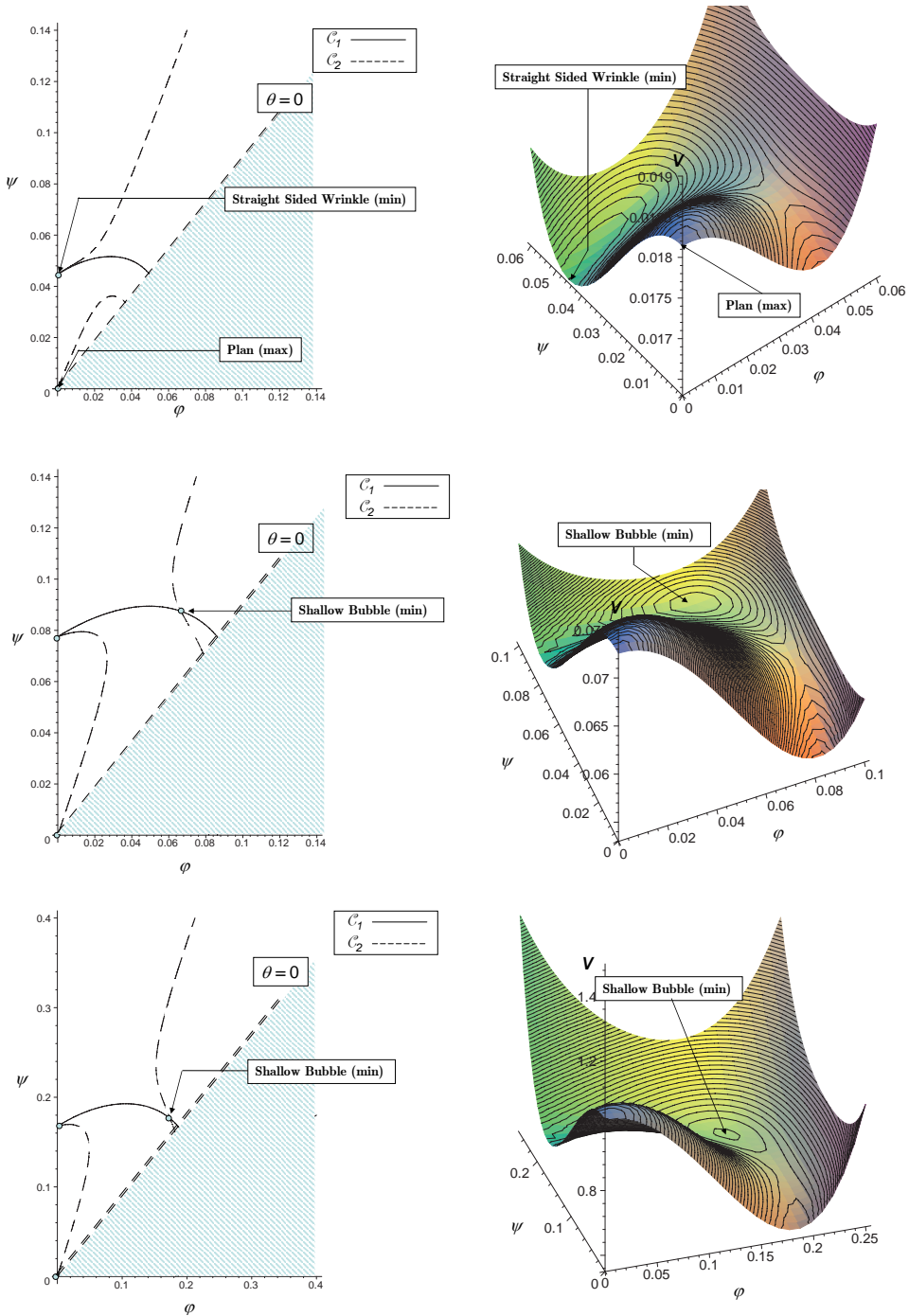


Figure 9. Equilibria for $a/b = 0.9$. Top: $\varepsilon = 0.002$; planar equilibrium ($\varphi = 0, \psi = 0$) and straight-sided equilibrium $\varphi = 0$ can be identified on the vertical axis. Middle: $\varepsilon = 0.004$; a stable shallow-bubble equilibrium arises, and the straight-sided equilibrium is unstable. Bottom: $\varepsilon = 0.015$; same equilibria as for $\varepsilon = 0.004$.

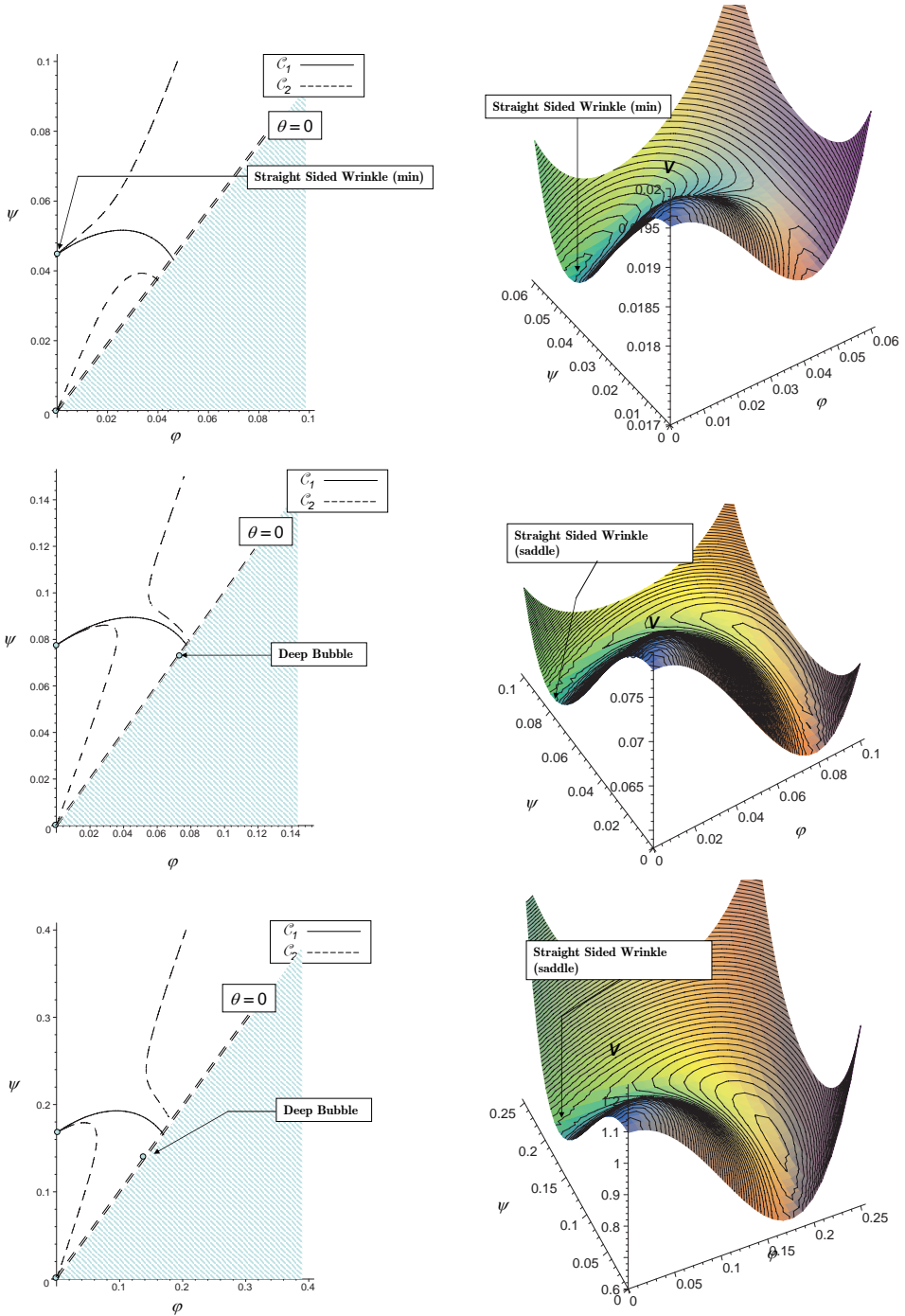


Figure 10. Equilibria for $a/b = 1$. Top: $\varepsilon = 0.002$; planar equilibrium ($\varphi = 0, \psi = 0$) and straight-sided equilibrium $\varphi = 0$ can be identified on the vertical axis. Middle: $\varepsilon = 0.004$; deep-bubble equilibrium is arising, and the other equilibria are unstable. Bottom: $\varepsilon = 0.015$; same observation as for $\varepsilon = 0.004$.

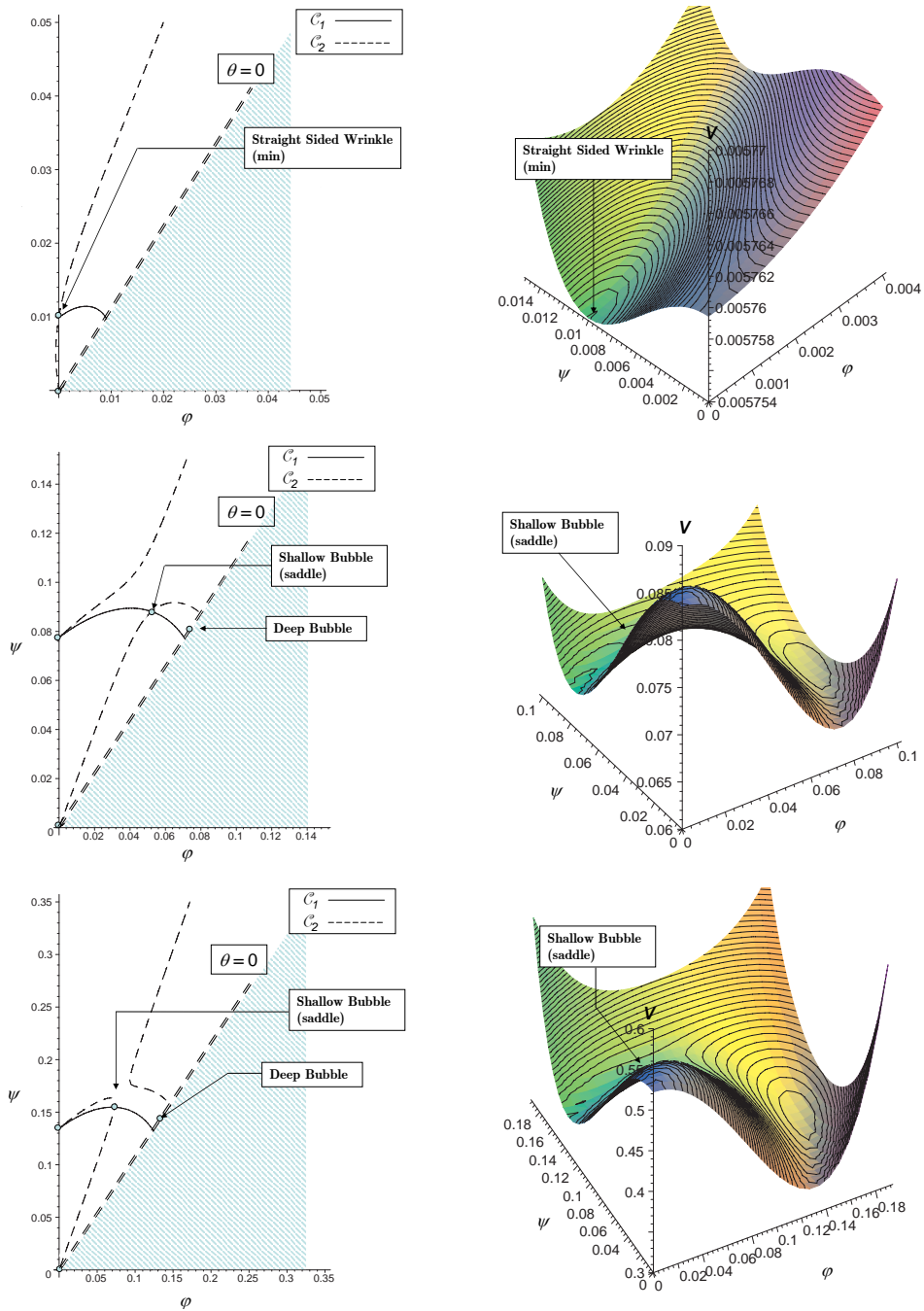


Figure 11. Equilibria for $a/b = 1.1$. Top: $\varepsilon = 0.001$; planar equilibrium ($\varphi = 0, \psi = 0$) and straight-sided equilibrium $\varphi = 0$ can be identified on the vertical axis. Middle: $\varepsilon = 0.004$; A shallow bubble equilibrium (unstable) and a deep bubble equilibrium are identified. Bottom: $\varepsilon = 0.010$. The same equilibria can be identified for higher deformation levels.

Short bubbles ($a/b = 0.9$). The case of short bubbles is illustrated in [Figure 9](#) for $a/b = 0.9$. A stable SB (shallow-bubble) equilibrium rapidly arises as the deformation level is raised. This buckling mode, characterized by values of φ that are rather small compared to ψ can be connected to experimental observations of small undulations (or incipient bubbles) on top of straight-sided wrinkles. It is experimentally observed that these undulations are short. As the deformation level ε increases, these undulations become deeper.

There is no deep-bubble equilibrium for this a/b ratio (no solution for the contact equilibrium problem). It is interesting to note that there are no experimental observations of short deep bubbles. We expect these to arise for higher levels of a/b .

Intermediate case ($a/b = 1$). For small values of the deformation ε ([Figure 10](#), top), the SSW (straight-sided wrinkle) equilibrium is stable. There is no other equilibrium, except the trivial flat equilibrium, which is unstable.

Over a critical value of the deformation, the SSW becomes unstable. The existence of a deep-bubble equilibrium arises simultaneously with this loss of stability ([Figure 10](#), middle and bottom). The potential energy of the DB (deep-bubble) equilibrium is lower than that of the SSW equilibrium, and in fact occupies the potential energy minimum. When losing its stability, the SSW will hence evolve toward a DB equilibrium. It is interesting to see, from the shape of the curves, that the transition cannot evolve smoothly. Because of the absence of a SB equilibrium, the structure cannot continuously evolve from SSW to DB. Snap-through is to be expected.

Longer bubbles ($a/b = 1.1$). The case $a/b \geq 1.1$ is illustrated in [Figure 11](#). For small values of ε , the SSW is the only nonplanar equilibrium (top) and is stable (at a potential energy minimum). As ε increases, an SB and a DB equilibria arise (middle and bottom), and the SSW loses its stability. The SB equilibrium is unstable and the system evolves to the DB equilibrium at the potential energy minimum.

It is worth noting that the SSW and the SB equilibria are close to each other in the (ψ, φ) space. Some defects on the wrinkle could trigger the shallow-bubble saddle-point mode in a transient way, which would lead to a snap-through to the deep-bubble equilibrium. This phenomenon has been observed both numerically and experimentally over a critical a/b ratio of the bubbles [[Parry et al. 2005](#)].

6. Conclusion

The results of this study clarify and give an explanation for various experimental observations of the post-critical buckling of delaminated films. First of all, some undulations are sometimes experimentally observed on the top of the straight-sided wrinkles ([Figure 2](#)). These undulations are short and shallow and neighbor areas with deep bubbles that are obviously longer. This is in agreement with the conclusion that the shallow bubbles equilibrium is stable for small values of a/b .

Experimental observations show that above a given length of the bubbles there is a transition between the straight-sided wrinkle and a bubble equilibrium where the edges of the bubbles are touching the substrate. It is also observed that for a critical value of a/b , between 1.1 and 1.2, the transition is subcritical [[Parry et al. 2005](#)]. This is in good agreement with the results of the rod model, both qualitatively and quantitatively, because it has been shown that for a critical value of the a/b ratio the shallow-bubble equilibrium becomes unstable and that the deep-bubble equilibrium is stable. If some undulations are

present on the top of the straight-sided wrinkle, due to defects or imperfections, the saddle-point shallow-bubble equilibrium can be briefly met immediately preceding the deep-bubble equilibrium with an abrupt transition.

The ability of this model to accurately represent the transitions in the post-critical regime of this buckling film system (qualitatively but also quantitatively, and with only a few variables) encourages further exploration and motivates work that will model the trigger behavior of plates and films for various post-critical regimes.

References

- [Abdallah et al. 2008] A. A. Abdallah, P. C. P. Bouten, J. M. J. Den Toonder, and G. de With, “The effect of moisture on buckle delamination of thin inorganic layers on a polymer substrate”, *Thin Solid Films* **516**:6 (January 2008), 1063–1073.
- [Arbocz et al. 1987] J. Arbocz, M. Potier-Ferry, J. Singer, and V. Tvergaard, *Buckling and post-buckling: four lectures in experimental, numerical and theoretical solid mechanics based on talks given at the CISM-Meeting held in Udine, Italy, September 29–October 3, 1985*, Lecture notes in physics **288**, Springer-Verlag, Berlin, 1987.
- [Audoly 1999] B. Audoly, “Stability of straight delamination blisters”, *Phys. Rev. Lett.* **83**:20 (1999), 4124–4127.
- [Coupeau et al. 1998] C. Coupeau, J. C. Girard, and J. Grilhe, “Plasticity study of deformed materials by in situ atomic force microscopy”, *J. Vac. Sci. Technol. B* **16**:4 (July 1998), 1964–1970.
- [Evans and Hutchinson 2007] A. G. Evans and J. W. Hutchinson, “The mechanics of coating delamination in thermal gradients”, *Surf. Coat. Technol.* **201**:18 (June 2007), 7905–7916.
- [Faulhaber et al. 2006] S. Faulhaber, C. Mercer, M.-W. Moon, J. W. Hutchinson, and A. Evans, “Buckling delamination in compressed multilayers on curved substrates with accompanying ridge cracks”, *J. Mech. Phys. Solids* **54**:5 (2006), 1004–1028.
- [George et al. 2002] M. George, C. Coupeau, J. Colin, F. Cleymand, and J. Grilhe, “Delamination of metal thin films on polymer substrates: from straight-sided blisters to varicose structures”, *Philos. Mag. A* **82**:3 (2002), 633–641.
- [Gille and Rau 1984] G. Gille and B. Rau, “Buckling instability and adhesion of carbon layers”, *Thin Solid Films* **120**:2 (1984), 109–121.
- [Gruttmann and Pham 2008] F. Gruttmann and V. D. Pham, “A finite element model for the analysis of buckling driven delaminations of thin films on rigid substrates”, *Comput. Mech.* **41**:3 (2008), 361–370.
- [Hutchinson and Suo 1991] J. W. Hutchinson and Z. Suo, “Mixed mode cracking in layered materials”, *Adv. Appl. Mech.* **29** (1991), 63–191.
- [Jagla 2007] E. A. Jagla, “Modeling the buckling and delamination of thin films”, *Phys. Rev. B* **75**:8 (2007), 085405.
- [Moon et al. 2004] M. W. Moon, K. R. Lee, K. H. Oh, and J. W. Hutchinson, “Buckle delamination on patterned substrates”, *Acta Mater.* **52**:10 (2004), 3151–3159.
- [Parry et al. 2005] G. Parry, J. Colin, C. Coupeau, F. Foucher, A. Cimetiere, and J. Grilhe, “Snapthrough occurring in the postbuckling of thin films”, *Appl. Phys. Lett.* **86**:8 (2005), 081905.
- [Parry et al. 2006] G. Parry, A. Cimetiere, C. Coupeau, J. Colin, and J. Grilhe, “Stability diagram of unilateral buckling patterns of strip-delaminated films”, *Phys. Rev. E* **74**:6 Pt 2 (2006), 066601.
- [Song et al. 2008] J. Song, H. Jiang, W. M. Choi, and D. Y. Khang, “An analytical study of two-dimensional buckling of thin films on compliant substrates”, *J. Appl. Phys.* **103**:1 (2008), 014303.
- [Thompson and Hunt 1973] J. M. T. Thompson and G. W. Hunt, *A general theory of elastic stability*, John Wiley, London, 1973.
- [Thouless et al. 1992] M. D. Thouless, J. W. Hutchinson, and E. G. Liniger, “Plane-strain, buckling-driven delamination of thin films: model experiments and mode-II fracture”, *Acta Metall. Mater.* **40**:10 (1992), 2639–2649.
- [Tvergaard and Hutchinson 2008] V. Tvergaard and J. W. Hutchinson, “Mode III effects on interface delamination”, *J. Mech. Phys. Solids* **56**:1 (January 2008), 215–229.

Received 8 Oct 2008. Revised 4 Dec 2008. Accepted 4 Dec 2008.

GUILLAUME PARRY: guillaume.parry@simap.grenoble-inp.fr

Laboratoire SIMaP/LTPCM, CNRS UMR 5266-INPG-UJF, 1130 Rue de la Piscine, 38402 Saint Martin d'Hères, France

CHRISTOPHE COUPEAU: christophe.coupeau@univ-poitiers.fr

Laboratoire de Metallurgie Physique (LMP), UMR 6630 du CNRS, Université de Poitiers, BP 30179, 86962 Futuroscope Cedex, France

JÉRÔME COLIN: jerome.colin@univ-poitiers.fr

Laboratoire de Metallurgie Physique (LMP), UMR 6630 du CNRS, Université de Poitiers, BP 30179, 86962 Futuroscope Cedex, France

ALAIN CIMETIÈRE: alain.cimetiere@univ-poitiers.fr

Laboratoire de Metallurgie Physique (LMP), UMR 6630 du CNRS, Université de Poitiers, BP 30179, 86962 Futuroscope Cedex, France